Fragmentation of CD$^+$ induced by intense ultrashort laser pulses

L. Graham,[1,2] M. Zohrabi,[3] B. Gaire,[3] U. Ablikim,[3] B. Jochim,[3] B. Berry,[3] T. Severt,[3] K. J. Betsch,[3] A. M. Summers,[3] U. Lev,[1] O. Heber,[1] D. Zajfman,[1] I. D. Williams,[2] K. D. Carnes,[3] B. D. Esry,[3] and I. Ben-Itzhak[3,*]

[1]*Department of Particle Physics, Weizmann Institute of Science, IL-76100 Rehovot, Israel*
[2]*School of Mathematics and Physics, Queens University Belfast, Belfast, BT7 1NN, United Kingdom*
[3]*J.R. Macdonald Laboratory, Physics Department, Kansas State University, Manhattan, Kansas 66506, USA*

The fragmentation of CD$^+$ in intense ultrashort laser pulses was investigated using a coincidence three-dimensional momentum imaging technique improved by employing both transverse and longitudinal electric fields. This allowed clear separation of all fragmentation channels and the determination of the kinetic energy release down to nearly zero, for a molecule with significant mass asymmetry. The most probable dissociation pathways for the two lowest dissociation limits, C$^+$ + D and C + D$^+$, were identified for both 22-fs, 798-nm and 50-fs, 392-nm pulses. Curiously, the charge asymmetric dissociation of CD^{2+} was not observed for 392-nm photons, even though it was clearly visible for the fundamental 798 nm at the same peak intensity.

I. INTRODUCTION

Innovative developments in ultrashort laser-pulse technology have led to the discovery of a plethora of fascinating laser-induced phenomena [1,2]. Amongst the most widely studied dissociation and ionization dynamics are bond softening [3,4], above threshold ionization (ATI) [5–9], above threshold dissociation (ATD) [4,10,11], and their control by the carrier-envelope phase of a few-cycle pulse [12–16]. Being the simplest molecular ion, the behavior of H$_2^+$ in intense laser fields has been extensively scrutinized to provide a comprehensive and intuitive insight into these dynamics and their dependence on pulse characteristics [17,18]. As this work is extended to more complex multielectron systems, the concepts are still applicable, but further questions regarding the interplay of different fragmentation channels arise.

In recent years, detection and imaging technologies have become increasingly sophisticated. The ability to perform kinematically complete measurements and identify fragmentation channels unambiguously has deepened our understanding of laser-ion interactions [15,16,19–28]. Heteronuclear molecules are an interesting subject for laser fragmentation studies due to their identifiable breakup channels, but they can present additional experimental challenges, especially as the mass ratio between the fragments increases.

In this paper, we present a version of our coincidence three-dimensional momentum imaging method modified to measure the dissociation channels of molecules with a significant mass asymmetry between the two fragments. To demonstrate the applicability of this piecewise approach, we employ it to study the dissociation channels of deuterated methylidyne cations, namely, CD$^+$ → C$^+$ + D and C + D$^+$. Moreover, these measurements take advantage of our ability to detect neutral fragments—an important benefit also in our studies of the C^{2+} + D products of dissociative ionization.

As acquiring the ability to drive chemical reactions using ultrafast lasers is one of our overarching goals, it is important to improve our understanding of the underlying mechanisms and provide a means to control the final products. The final products of CD$^+$ dissociation, the subject of this study, are distinguishable, therefore helping one to determine the dissociation mechanisms leading to each of them, as well as their relative importance. Previous studies explored the dissociation of other mass asymmetric molecules, such as ND$^+$ and DCl$^+$ [29,30]. The energy separation between the lowest two dissociation limits in both of those cases is less than one 798-nm photon. In contrast, the energy gap between the lowest two dissociation limits of CD$^+$, namely, the C$^+$ + D and C + D$^+$, is larger than one 798-nm photon. Therefore, excitations require multiphoton transitions.

At intensities high enough to drive multiphoton transitions in a molecule, it is convenient to use the Floquet representation to conceptually visualize the dynamics of the system in the laser field [17,18]. In the diabatic representation of this picture, the electronic states are shifted by multiples of the photon energy $\hbar\omega$, which causes them to cross. At these crossings, transitions between the states are most likely to occur, assuming the transition dipole coupling is sufficient. However, the diabatic Floquet picture of most molecules is incredibly complex due to the abundance of laser-induced crossings, making the unambiguous determination of laser-induced dissociation pathways a nontrivial task. A method for identifying the dissociation path using a process of elimination has been described by Sayler *et al.* [31]. This method takes advantage of all the information measured starting from the identification of the final products C$^+$ + D and C + D$^+$ in our case, through the measured kinetic energy release (KER), the angular distribution, and the wavelength and intensity dependence of the spectra. In addition, dipole selection rules help reduce the number of possible transitions significantly. This technique is further described in Sec. III and employed to determine the most probable dissociation pathways leading to the two lowest dissociation limits of CD$^+$, namely, C$^+$ + D and C + D$^+$.

The charges of a multiply charged molecular ion can either be shared evenly amongst the fragments, as is the case for

*Also at Department of Particle Physics and Astrophysics, Weizmann Institute of Science, Rehovot, Israel (Weston Visiting Professor).

charge-symmetric dissociation (CSD), or unequally in a process termed charge-asymmetric dissociation (CAD) [32,33]. The occurrence of CAD has been experimentally confirmed and explored in great detail [32–41]. However, the mechanism by which CAD states are initially populated are far from understood. These states lie substantially higher in energy than the CSD states, and a dispute remains as to whether or not these states are populated via a charge transfer transition from the corresponding CSD states. Additional work on CAD has reported a strong dependence on the duration of the laser pulse driving this less-likely fragmentation channel [34,38,42].

In Sec. II, we demonstrate an extension of our coincidence three-dimensional (3D) momentum imaging method to molecular ions with significant mass asymmetry between the two fragments, which goes way beyond our ND^+ work [29]. Employing this method, we study the breakup of CD^+ in intense, ultrashort (22 fs at 798 nm and 50 fs at 392 nm) laser pulses. Using the measured KER and angular distributions, we determine the most likely dissociation pathways, as discussed in Sec. III A. Following Sec. III A, we briefly discuss the relative importance of the two lowest dissociation channels. Finally, in Sec. III B we explore the CAD of CD^{2+}, namely, the breakup into $C^{2+} + D$—which, surprisingly, is not observed for 392-nm photons at the same peak intensity as the fundamental 798 nm, for which CAD is observed.

II. EXPERIMENTAL METHOD

The experimental method employed in this work is a modified version of the one used in our earlier studies of laser–molecular-ion interactions [21,43,44]. In a nutshell, this method allows the measurement of all beam fragments, including neutral fragments but not including electrons, in coincidence and provides a complete 3D momentum image of all fragments. Moreover, the different fragmentation channels are experimentally distinguishable. The fragmentation of the molecular-ion beam is induced by the strong field of ultrashort laser pulses crossing the ion beam in the interaction region of the apparatus shown schematically in Fig. 1(a).

In the present study we used a high repetition rate (10 kHz) Ti:sapphire laser system, which we call PULSAR. It had a fundamental wavelength of 798 nm and provided linearly polarized 22($\pm$2) fs [full width at half maximum (FWHM) of intensity, as determined by a frequency resolved autocorrelation (FRAC) measurement [45,46]] Fourier transform limited (FTL) pulses with up to 2 mJ energy [47]. The high power PULSAR beam diameter was reduced by a factor of about 2.2 (from 40 to 18 mm diameter) using (in reverse) a reflective beam expander in order to match the standard 1 inch optics in our setup. The laser beam was finally focused onto the ion-beam target by an $f = 203$ mm off-axis parabolic mirror. The laser polarization was usually set along the ion-beam direction in order to reduce the spot size of the molecular fragments hitting the detector. This is made possible by the fact that most molecular-breakup processes favor alignment parallel to the laser field [17,18].

Second harmonic pulses at 392 nm (measured-spectrum centroid) were used for some of the measurements. In this case the 392-nm beam was produced via nonlinear sum-frequency generation inside a β-barium borate (BBO) crystal [48,49]. To
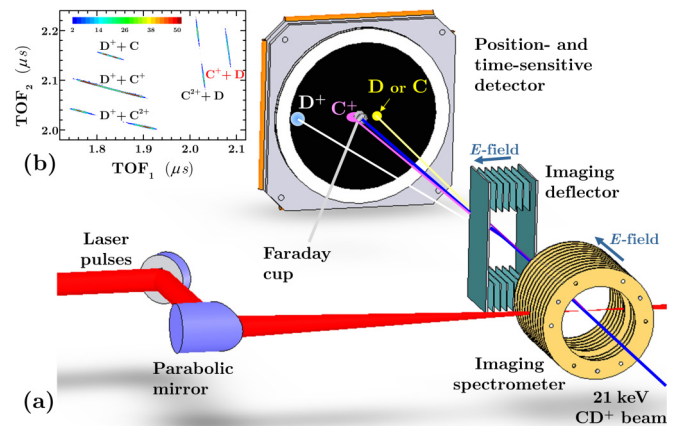

FIG. 1. (Color online) (a) Schematic of the experimental setup. (b) Coincidence time of flight map of CD^+ fragmentation in 22-fs, 798-nm and 6.3×10^{15} W/cm^2 laser pulses, which shows distinguishable breakup channels of CD^+. Most of the breakup channels were measured with low voltage on the deflector, while the $C^+ + D$ channel (pink label) was measured with high voltage on the deflector (see Sec. II).

improve the conversion efficiency in the BBO, the diameter of the 798-nm laser beam was further reduced by a factor of 2 using another reflective beam expander. Then, the output light from the BBO was separated using a dichromatic beam splitter that transmits the 392-nm light and reflects the 798-nm light. Finally, the resulting 392-nm beam was expanded, by a factor of 2 in yet another reflective beam expander, to allow for tighter focusing and higher peak intensities in measurements employing the second harmonic. The pulse duration was measured by a self-diffraction frequency resolved optical gating (SD-FROG) apparatus to be 50 fs (positively chirped from the 34-fs FTL pulse supported by the bandwidth, which is significantly narrower than the bandwidth of the 798-nm pulse due to the nonlinear second-harmonic generation mechanism) with a peak intensity up to 6.4×10^{14} W/cm^2.

A collimated, mass selected, 21-keV CD^+ ion beam served as the target in our present measurements. This CD^+ beam was crossed perpendicularly with the focused laser beam in the interaction region, located inside a spectrometer providing a 400-V/cm electric field along the ion-beam direction, as shown in Fig. 1(a). This field separates the fragments in time of flight according to their charge and mass, therefore allowing us to distinguish the different fragmentation channels, as shown in Fig. 1(b). After the interaction the ion beam was monitored for normalization by a small movable Faraday cup (2 mm diameter), which also acts to protect the imaging detector. If no transverse electric field is applied on the "imaging deflector," then only molecular fragments that make it past the Faraday cup, due to the transverse momenta they gain during the fragmentation process, can be detected in coincidence by the imaging detector. The detector used consists of a microchannel plate assembly (chevron) coupled with a delay-line-anode readout and operated in an event-by-event mode. The three-dimensional momenta of both molecular fragments were evaluated from the measured time and position of both hits. Using this momentum information, the KER and angular

distributions of each breakup channel were determined (see additional experimental details in our previous publications, e.g., [21,43,50,51]).

The main drawback of the setup described above is, as mentioned, that it is limited to measurements of fragments that have sufficient transverse momentum to clear the Faraday cup used to collect the ion beam. This limitation has been alleviated by adding a transverse electric field to separate the detected particles by their position on the detector [52]. It has been shown that the additional static field does not degrade the resolution of this imaging technique [52]. More importantly, the transverse field, shown in Fig. 1(a), can be set to direct the low-KER fragments off the Faraday cup, thus enabling their detection. This technique was employed by Gaire *et al.* [20] to study the dissociation of D$_3^+$ down to near zero KER (limited to about ~ 0.8 meV only by the detector resolution).

In a followup work Gaire *et al.* [53] studied the ratio of nondissociating ionization to dissociative ionization of CO$^+$, namely, the competition between the CO^{2+} and C$^+$ + O$^+$ channels, taking advantage of the distinct trajectory of the different ions.

In the present work we demonstrate that this transverse field improves coincidence 3D momentum imaging measurements of mass asymmetric heteronuclear molecules. For these systems, the massive fragment might have a very small transverse velocity in comparison to the light fragment, and as a result it is likely to end up in the Faraday cup when the transverse momentum of the fragment is low. In contrast, for fragments with high transverse momenta, the light fragment may miss the detector. For example, such losses were the main limiting factor in previous measurements of laser-induced dissociation of ND$^+$ conducted with the longitudinal field only [29], in contrast to data acquired with both longitudinal and transverse fields [52].

As a result of the losses discussed above, coincidence 3D momentum imaging measurements of mass asymmetric molecular ions require special care, as the transverse field that allows the measurement of one fragmentation channel might not be ideal for other channels. To design the best conditions for measuring the CD$^+$ breakup channels of interest in this work, namely, C + D$^+$, C$^+$ + D, and C^{2+} + D, we simulated the position distributions of all the fragments assuming that the dissociation occurs in the detector plane, which is the

alignment causing the largest spot on the detector for a given KER. To make the simulations realistic we used the most likely KER value of each channel as determined by preliminary measurements. Specifically, these are 0.5 eV for both dissociation channels and 2.3 eV for the C^{2+} + D breakup channel. These simulations, shown in Figs. 2(a) and 2(e), suggest that all the channels of interest mentioned above can be measured using two transverse field values. Specifically, a transverse field of 39.3 V/cm is ideal for measuring the C + D$^+$ and C^{2+} + D breakup channels, as shown in Fig. 2(a). However, under these conditions most of the C$^+$ fragments from C$^+$ + D dissociation are lost in the Faraday cup. Using a stronger transverse field of 170 V/cm enables the measurement of the C$^+$ + D dissociation channel, as shown in Fig. 2(e), but in this case the C + D$^+$ and C^{2+} + D events are lost, as the D$^+$ and C^{2+} fragments are deflected off the detector. Note that these measurements are made easier by directing the primary beam off the detector center (by 10.5 mm), thus making the detector effectively larger.

For our CD$^+$ test case, the simulation results were verified by the measured position distributions of both fragments of each breakup channel, shown as scatter plots in Figs. 2(b)–2(d). It can clearly be seen that losses are minimized for the C + D$^+$ and C^{2+} + D breakup channels measured with the weak field of 39.3 V/cm [panels (b) and (c)], and for the C$^+$ + D dissociation channel measured with the stronger 170 V/cm field [panel (d)]. A careful inspection of the measured position distributions shown in Fig. 2(d), however, indicates that some C$^+$ fragments (from C$^+$ + D) are lost as they move down (toward the Faraday cup). These losses can be recovered by taking advantage of the cylindrical symmetry around the laser polarization that is pointing along the ion-beam axis.

One consequence of this piecewise-measurement technique is that it requires a good method for normalizing the two data sets to each other. As a result, it is less accurate than the simultaneous measurement of different breakup channels, when such a measurement is possible. Another drawback of this method is the need for doubling the measurement time, not an insignificant price for these typically long measurements. To compare the independently measured C$^+$ + D and C + D$^+$ dissociation channels to each other, the two measurements are normalized by matching the number of molecular ions exposed
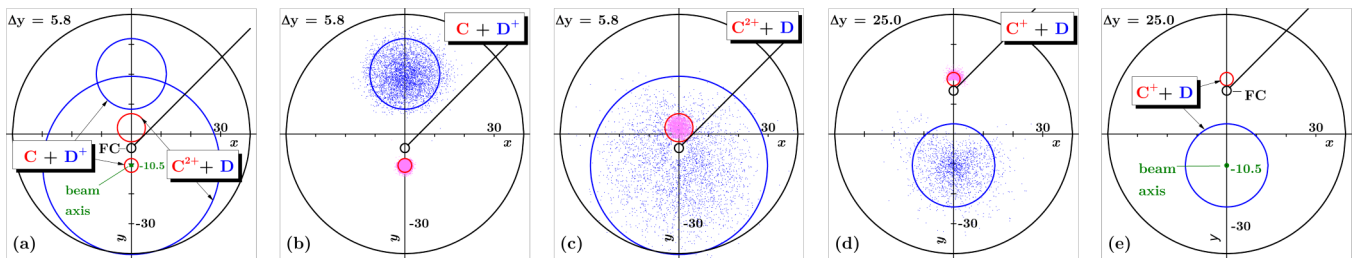

FIG. 2. (Color online) The simulated [(a),(e)] and measured [(b)–(d)] positions of the different CD$^+$ fragments on the imaging detector employing weak [39.3 V/cm, (a)–(c)] and strong [170 V/cm, (d) and (e)] transverse electrostatic fields. The scatter plots shown in panels (b)–(d) were measured with 22-fs, 798-nm and 6.3×10^{15} W/cm^2 laser pulses. The blue lines and dots are associated with deuterium fragments, while the red lines and magenta dots are associated with the carbon fragments. The Faraday cup is denoted by FC and the value of Δy in each panel indicates the deflection of the CD$^+$ beam spot (marked by FC on the detector) from the beam axis (all dimensions in the figure are in millimeters). Recall that the ion beam is pointing into the page.

to the laser pulses. This number, N, is given approximately by

$$N = \frac{A}{wv_B q} \int_0^T f(t)i(t)dt, \tag{1}$$

where A is the interaction area, i.e., the overlap between the laser and ion beams, w is the ion-beam width (typically about 0.8 mm), v_B is the ion-beam velocity, and q is the ion charge. Inside the integral, $i(t)$ is the ion-beam current and $f(t)$ is the laser repetition rate, monitored by the Faraday cup and a photodiode, respectively, and T is the duration of each measurement. To reduce the error introduced by this normalization procedure, the two measurements were conducted consecutively, switching only the transverse-field strength while keeping the laser and ion-beam parameters fixed. This leads to a normalization factor of $F = [\int_0^{T'} f'(t)i'(t)dt]/[\int_0^T f(t)i(t)dt]$, in which the main source of uncertainty is the laser stability over the long measurements needed—estimated to be about 10%–20% by reproducing a few measurements.

Finally, it is important to note that the CD^+ beam is produced in an electron cyclotron resonance (ECR) ion source by fast electron impact ionization of CD_4 gas. The CD^+ ions arrive at the interaction region with the laser in a combination of the electronic ground state, $X\,^1\Sigma^+$, and the lowest triplet state, namely, the $a\,^3\Pi$, which has a lifetime of a few seconds [54]—much longer than the few tens of microseconds flight time through our apparatus. This long-lived triplet state may constitute about half the CD^+ beam [54,55]. Moreover, the vibrational distribution in both electronic states is possibly vibrationally "hot" [56] and may affect the outcome of the laser interaction with the CD^+ molecular ions. The approximate vibrational population distribution is evaluated in Sec. III employing the Franck-Condon principle, which is expected to be valid for fast electron impact ionization.
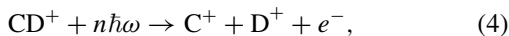
III. RESULTS AND DISCUSSION

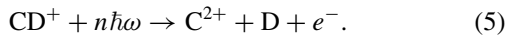Dissociation of a CD^+ target in a strong laser field leads to two final products that we can distinguish, namely,

$$CD^+ + n\hbar\omega \rightarrow C^+ + D, \tag{2}$$

and

$$CD^+ + n\hbar\omega \rightarrow C + D^+. \tag{3}$$
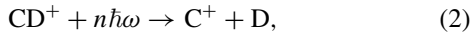
In addition, dissociative ionization of the CD^+ target may result in rapid fragmentation into

$$CD^+ + n\hbar\omega \rightarrow C^+ + D^+ + e^-, \tag{4}$$

i.e., the CSD channel. Alternatively, the CD^{2+} can also undergo a charge asymmetric dissociation, namely,

$$CD^+ + n\hbar\omega \rightarrow C^{2+} + D + e^-. \tag{5}$$

In the reactions above, $n\hbar\omega$ denotes the multiphoton interaction with the strong laser field. Also, note that electrons are not detected.

Since the mass asymmetry makes it difficult to measure the $C^+ + D^+$ channel, we focus our discussion on the other three channels listed above. Our measurements were conducted with 22-fs, 798-nm laser pulses at intensities ranging from 7.7×10^{12} W/cm² to 6.3×10^{15} W/cm², and 50-fs,
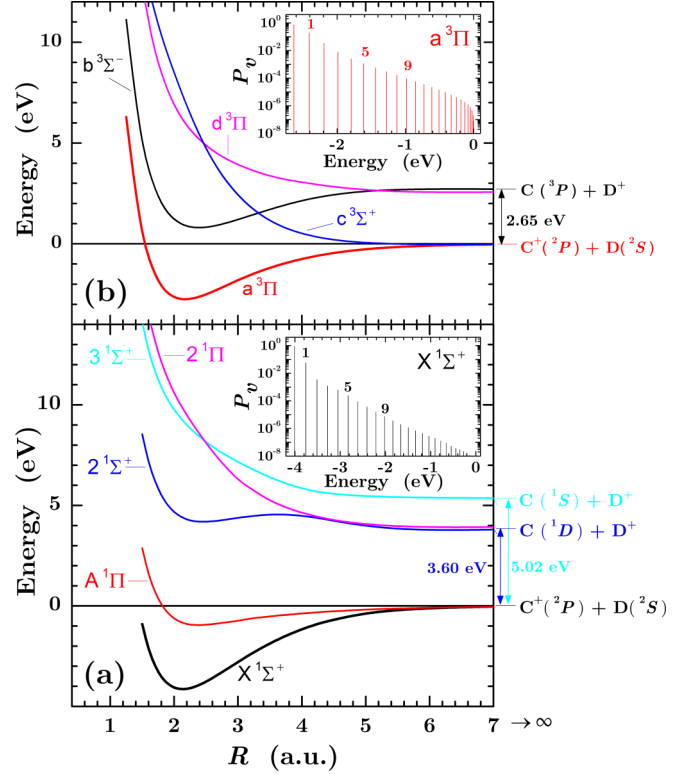

FIG. 3. (Color online) Lowest few potential energy curves (PECs) of CD^+ (assumed to be the same as the ones reported in literature for CH^+ [57–59]): (a) singlet states from Ref. [58], and (b) triplet states from Ref. [59] except the $c\,^3\Sigma^+$ state, which is from Ref. [57]. Note that the energy in each panel is given relative to the lowest dissociation limit of this group of states. The computed vibrational population of the $X\,^1\Sigma^+$ and $a\,^3\Pi$ states of CD^+ are shown as insets in panels (a) and (b), respectively.

392-nm laser pulses with 1.5×10^{13} to 6.4×10^{14} W/cm² peak intensity. For simplicity, we only show a sampling of these data.

As mentioned in Sec. II, the target CD^+ ions originating from the ion source are most likely vibrationally excited. The possible dissociation path in the strong laser field also depends on the initial vibrational state, as will be shown later. The vibrational populations in the lowest singlet and triplet states—both present in the ion beam—are shown in the insets of Fig. 3. These populations were determined approximately by evaluating the Franck-Condon factors, specifically

$$\mathcal{F}_{fi} = \left| \int_0^\infty \psi_f(R)\psi_i(R)dR \right|^2, \tag{6}$$

where R is the C-D internuclear distance. The vibrational wave functions, $\psi_f(R)$, bound in the $X\,^1\Sigma^+$ or $a\,^3\Pi$ states, were computed using a phase-amplitude method [60]. The initial nuclear wave function along the CD bond in methane was modeled as the ground state wave function of the simple harmonic oscillator centered around the C-D bond length, $R_0 = 2.07$ a.u. [61], with the fundamental frequency for symmetric C-D stretch, $\omega_0 = 2084.7$ cm⁻¹ [62,63]. In this calculation, we neglected the decay of excited singlet and triplet states, all expected to decay before reaching

the interaction region, because electron impact ionization preferentially populates lower-energy states.

A. Dissociation pathways

The coincidence 3D momentum imaging technique employed in this study provides information about the dissociation channels that goes beyond the measured yields discussed above. As a typical example, we show in Fig. 4 the KER and KER-$\cos\theta$ distributions measured with the highest intensity fundamental IR (798 nm, 22 fs, 6.3×10^{15} W/cm^2) and second harmonic (392 nm, 50 fs, 6.4×10^{14} W/cm^2) pulses. The shape of these measured distributions does not change significantly with laser intensity. Importantly, there is a notable difference between the KER distribution of the two dissociation channels. Specifically, the $C^+ + D$ breakup yields lower KER values than the $C + D^+$ channel. The reason for this difference stems from the different shape of the final-state
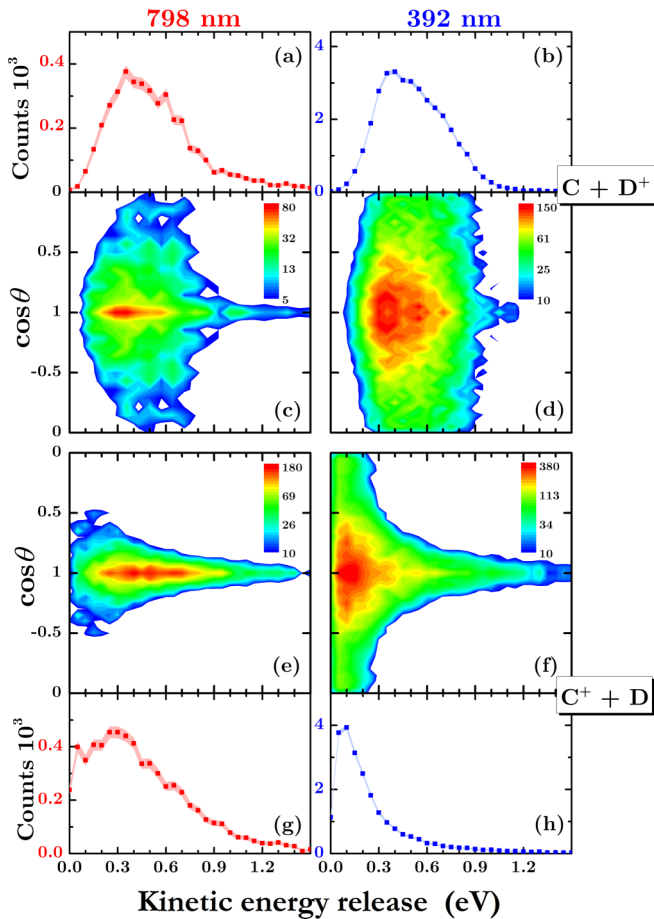

FIG. 4. (Color online) The measured KER and angular distributions for $C + D^+$ [(a)–(d)] and $C^+ + D$ [(e)–(h)] dissociation at the highest intensity, 6.3×10^{15} W/cm^2 and 6.4×10^{14} W/cm^2 for the fundamental IR (798 nm, 22 fs), and second harmonic (392 nm, 50 fs), respectively, as labeled on the panels (KER-$\cos\theta$ density plot [(c)–(f)] and KER distributions integrated over all angles [(a),(b), and (g),(h)]). Note that in the former the measured data for $\cos\theta > 0$ were reflected about zero to reduce the impact of fragment losses, and in the latter the shaded areas about the measured distributions represent statistical errors.
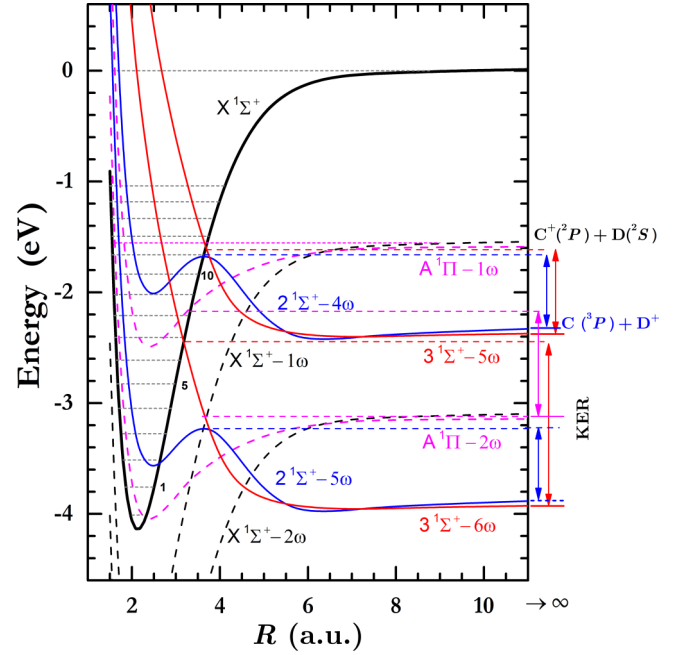

FIG. 5. (Color online) Light-dressed-states diagram of a few potential energy curves of CD⁺ singlet states (taken from Fig. 3) relevant to the dominant dissociation pathways leading to $C^+(^2P) + D(^2S)$ [$X\,^1\Sigma^+$ and $A\,^1\Pi$ states—dashed lines] and $C(^3P) + D^+$ [$2\,^1\Sigma^+$ and $3\,^1\Sigma^+$ states—solid lines] (see text). Dissociation pathways involving the 392 nm are denoted by 2ω, 4ω, and 6ω, where ω is the energy of the 798-nm photon [66]. The electronic states are indicated by color as follows: $X\,^1\Sigma^+$ (black), $2\,^1\Sigma^+$ (blue), $3\,^1\Sigma^+$ (red), and $A\,^1\Pi$ (magenta).

PEC along the dissociation path associated with each channel as explained below.

To determine which dissociation pathways are the most likely ones, we follow the method described in detail in Ref. [31]. In a nutshell, we search for dissociation paths consistent with the measured KER, angular distribution, intensity dependence, etc. It is convenient to discuss the dissociation pathways using a light-dressed-states (Floquet) diagram [64,65], shown for CD⁺ dissociation in Fig. 5. The potential curves of the relevant singlet states of CD⁺, from Ref. [58] (the $2\,^1\Pi$ state was omitted for simplicity as we have found no likely dissociation pathway involving this state), are the same as the ones shown in Fig. 3, but in the light-dressed-states picture each potential curve is labeled by the number of 798-nm photons absorbed. For example, the $2\,^1\Sigma^+$ state dressed by four photons is labeled in Fig. 5 as $2\,^1\Sigma^+ - 4\omega$.

Where curves cross one another, transitions from one state to the other are most likely. The rate of these transitions depends on the magnitude of the transition dipoles, which are expected in most cases to drop exponentially above $R = 7$, i.e., where the PECs become flat. In some cases, like $X\,^1\Sigma^+$ to $A\,^1\Pi$ transitions, the transition dipoles are expected to become constant asymptotically. However, as the molecular dynamics are expected to occur around the light-dressed curve crossings along the dissociation paths, shown in Figs. 5 and 6, dipole coupling should not be negligible at $R < 7$. To treat the
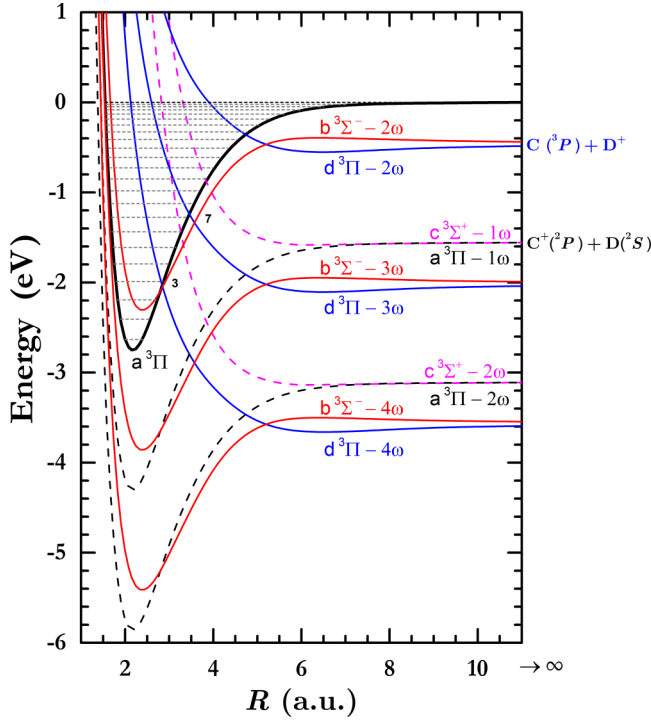
FIG. 6. (Color online) Light-dressed-states diagram of a few potential energy curves of CD^+ triplet states (taken from Fig. 3) relevant to the dissociation pathways leading to $C^+(^2P) + D(^2S)$ [$a\,^3\Pi$ and $c\,^3\Sigma^+$ states—dashed lines] and $C(^3P) + D^+$ [$b\,^3\Sigma^-$ and $d\,^3\Pi$ states—solid lines] (see text). Dissociation pathways involving the 392 nm are denoted by 2ω and 4ω, where ω is the energy of the 798-nm photon [66]. The electronic states are indicated by color as follows: $a\,^3\Pi$ (black), $c\,^3\Sigma^+$ (magenta), $b\,^3\Sigma^-$ (red), and $d\,^3\Pi$ (blue).

dissociation of CD^+ theoretically, these transition coupling matrix elements will need to be calculated.

Using the dressed states in Figs. 5 and 6, the KER can easily be estimated by evaluating the difference in energy between the initial energy and the final dissociation limit. For example, a few KER values relevant to the current work are marked by the vertical arrows in Fig. 5. However, we emphasize that these energies will only be approximate as bond softening and ATD [3,4,10], etc., can lead to dissociation of vibrational states above and below the initial crossing, which in turn leads to higher and lower KER values observed, respectively.

Finally, before discussing the dissociation paths leading to $C^+ + D$ and $C + D^+$ in detail, it is worth comparing their relative importance. Using the 392-nm measurements at 2.0×10^{13} W/cm^2 as an example, we evaluated the branching ratio $N(C^+ + D)/[N(C^+ + D) + N(C + D^+)]$ to be 0.39 ± 0.14, which suggests that the two channels are comparable at this intensity. It is important to note that the main source of the uncertainty is the lost C^+ and D^+ fragments due to the Faraday cup and detector edge, respectively. One should also consider the meaning of this branching ratio given the fact that the CD^+ investigated is initially in an unknown mix of the $X\,^1\Sigma^+$ electronic ground state and the long-lived $a\,^3\Pi$ triplet state. To further explore the branching ratios, it is advisable to determine the relative initial population in these two states.

1. Dissociation pathways leading to $C^+ + D$

As mentioned earlier, the laser field does not couple states of different spin multiplets. The fact that spin-orbit coupling, which may couple such states, occurs on a much slower time scale allows us to consider separately the dissociation pathways of the $X\,^1\Sigma^+$ and $a\,^3\Pi$ states present in the CD^+ beam [54,55].

Singlet states. The fact that the KER distribution of this breakup channel extends to 0 eV and rapidly falls off with increasing KER for both the 798- and 392-nm pulses is consistent with the dissociation pathway $|X\,^1\Sigma^+(v \geqslant 4) - 0\omega\rangle \rightarrow |A\,^1\Pi - 2\omega\rangle$, where ω is the fundamental frequency. Note that the dissociation of $v < 4$ states by this process is energetically forbidden, as indicated in Fig. 5, and the KER distribution peaking at zero KER is typical for final bound states, like the $A\,^1\Pi$ [31]. For the 798-nm pulse, highly excited vibrational states bound in the $X\,^1\Sigma^+$ potential well can also dissociate through one-photon absorption, namely, $|X\,^1\Sigma^+(v \geqslant 12) - 0\omega\rangle \rightarrow |A\,^1\Pi - 1\omega\rangle$, yielding an overlapping KER distribution. Even though the latter pathway requires only one-photon absorption instead of two, the fact that the initial population of these highly excited vibrational states is about three orders of magnitude lower reduces the importance of this dissociation route. The fact that the 2ω pathway dominates for the IR is the reason for the similarity of its KER spectrum to that of the second harmonic. The higher dissociation rate with 392 nm (by a factor of about 6 at a somewhat lower intensity) is a consequence of being a one-photon process in contrast to two required at 798 nm.

Triplet states. The main dissociation path identified $|a\,^3\Pi(v \sim 7\text{--}10) - 0\omega\rangle \rightarrow |d\,^3\Pi - 3\omega\rangle \rightarrow |a\,^3\Pi - 1\omega\rangle$, shown in Fig. 6, is consistent with the dominant KER feature extending from 0.25 to 0.75 eV in Fig. 4(e). All the transitions along this dissociation path are parallel (i.e., $\Delta\Lambda = 0$), therefore resulting in strong alignment along the laser polarization. Moreover, the fact that the net number of 798-nm photons involved in these transitions is odd excludes it from the second harmonic measurements, which explains why we do not observe this dominant feature in the 392-nm data shown in Fig. 4(f). The long aligned KER tail, extending from about 0.5 to 1.4 eV and visible in both 798- and 392-nm data, is consistent with the $|a\,^3\Pi(v \sim 0\text{--}3) - 0\omega\rangle \rightarrow |d\,^3\Pi - 4\omega\rangle \rightarrow |a\,^3\Pi - 2\omega\rangle$ dissociation path.

2. Dissociation pathways leading to $C + D^+$.

Singlet states. The similarity of the KER distributions of this breakup channel measured with 798 nm and 392 nm—both peaking near 0.3–0.4 eV—suggests that the dissociation pathway is similar. The most likely dissociation pathway is identified to be $|X\,^1\Sigma^+(v \sim 11) - 0\omega\rangle \rightarrow |2\,^1\Sigma^+ - 4\omega\rangle$. Here, too, the dissociation rate with 392 nm is higher than for 798 nm (by about a factor of 3) because of the lower number of photons required. As indicated in Fig. 5, the dissociation pathway $|X\,^1\Sigma^+(v \sim 11) - 0\omega\rangle \rightarrow |3\,^1\Sigma^+ - 5\omega\rangle$ should also peak at a similar KER value; however, this dissociation path is not possible for 392-nm photons. In contrast, the $|X\,^1\Sigma^+(v \sim 7) - 0\omega\rangle \rightarrow |3\,^1\Sigma^+ - 6\omega\rangle$ dissociation pathway is open for both 798 and 392 nm, but it leads to a KER of about 1.5 eV for the 392 nm (marked in Fig. 5 by a long red arrow).

This KER value is much higher than the measured value, thus suggesting that it is not an important dissociation pathway in this case. Another dissociation path, shown in Fig. 5, which can contribute only to the KER distribution measured with 798-nm photons, is $|X\,^1\Sigma^+ (v \sim 3) - 0\omega\rangle \rightarrow |2\,^1\Sigma^+ - 5\omega\rangle$. The KER distribution for this dissociation path is expected to extend to lower KER values, and it is observed in the measured KER spectrum for 798 nm shown in Fig. 4(a). This dissociation path requires the absorption of one additional photon compared to the dominant path discussed above, but the initial vibrational population is much higher, so it is not surprising that it can be observed in the KER spectrum. Note that all these dissociation paths yielding $C + D^+$ involve $\Delta\Lambda = 0$ (i.e., $\Sigma^+ \rightarrow \Sigma^+$) transitions and therefore are expected to favor fragmentation along the laser polarization [31,67], which is the measured angular preference suggested by Fig. 4(c). Finally, the KER distribution peaks around 0.5 eV, which is the value expected for dissociation pathways involving the $2\,^1\Sigma^+$ state because this is the energy of the top of its potential barrier with respect to the $C + D^+$ dissociation limit. Some of the vibrational states quasibound within this potential well can still dissociate, either by tunneling or by suppression of the barrier by the laser field, but at a lower rate.

Triplet states. The $C + D^+$ final products can also be reached by dissociation of the long-lived $a\,^3\Pi$ state present in the CD^+ beam [54,55]. The main path leading to low-KER $C + D^+$ breakup, shown in Fig. 6, is $|a\,^3\Pi(v \sim 15) - 0\omega\rangle \rightarrow |d\,^3\Pi - 2\omega\rangle$, and it can occur for both the fundamental and second harmonic. The resulting angular distribution of these parallel transitions is expected to be aligned along the laser polarization, but tighter for the 798 nm than the 392 nm as it is a two-photon transition for the former and only one for the latter—a result consistent with the data shown in Figs. 4(c) and 4(d). The data shown in these figures also suggest contributions from dissociation involving perpendicular transitions (i.e., $\Delta\Lambda = 1$). The dissociation path $|a\,^3\Pi(v \sim 15) - 0\omega\rangle \rightarrow |b\,^3\Sigma^- - 2\omega\rangle$ may be the source for those, again for both wavelengths used.

B. Charge asymmetric dissociation (CAD)

As mentioned in Sec. III, the CD^{2+} ion, formed by single ionization of the CD^+ target in our case, can dissociate to $C^+ + D^+$ or $C^{2+} + D$. The former, having a symmetric charge-state distribution [see Eq. (4)], is usually the dominant dissociative ionization channel (see, e.g., the review by Codling and Frasinski [68] and Refs. [33,44,69–73]). The latter, in contrast, has an asymmetric charge state distribution [CAD; see Eq. (5)], and this weak CAD channel has, by comparison, been studied less extensively [32–34,36,74].

Calculating the PECs for the high lying CAD states of a molecule is a nontrivial task. As a result, such information is scarce. Fortunately, *ab initio* calculations of the relevant states of CD^{2+} exist, and the adiabatic PECs computed by Gu *et al.* [75] are shown in Fig. 7. Inspection of Fig. 7 indicates that the lowest dissociation limits for CSD channels are significantly lower in energy as compared to the lowest CAD channel. Typically, some of the CSD states cross the CAD state at specific internuclear distances, which we denote R_c herein (see Fig. 7). Several authors have reported a strong
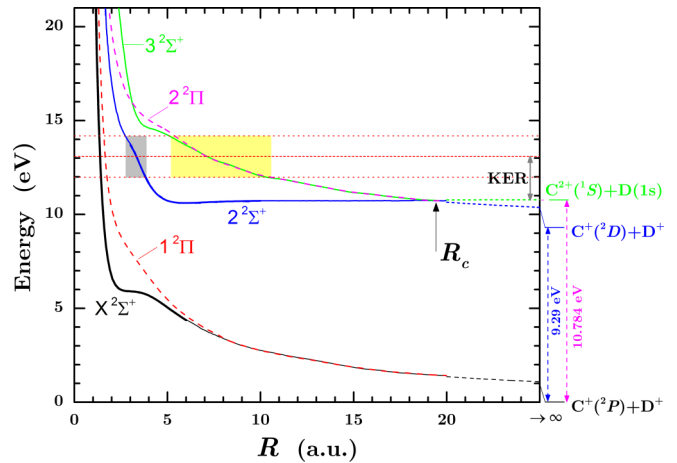

FIG. 7. (Color online) Lowest few potential energy curves of CH^{2+} from Ref. [75]. Note the avoided crossing between the $2\,^2\Sigma^+$ and $3\,^2\Sigma^+$ at $R_c = 19.4$ a.u. (indicated by an arrow). It is the $3\,^2\Sigma^+$ state which correlates to the $C^{2+} + D$ dissociation limit (green tic mark) [75]. The measured KER spread is marked by the horizontal red dotted lines, where the middle line signifies the average KER. The corresponding internuclear distances (hence R_i), estimated assuming no KER is gained prior to ionization to the $2\,^2\Sigma^+$ (gray) and the $3\,^2\Sigma^+$ and $2\,^2\Pi$ (yellow) states, are marked by the shaded areas.

avoided crossing between the $2\,^2\Sigma^+$ and $3\,^2\Sigma^+$ states of CD^{2+} [75–77]. However, there are discrepancies about the exact internuclear distance R_c at which this occurs. Most recently, Gu *et al.* [75] reported an avoided crossing at $R_c = 19.4$ a.u., which is by comparison considerably larger than for CAD channels studied in other molecules, such as N_2, I_2, and CO [32,34,68]. Provided the coupling is strong enough, CAD dissociation channels can be populated or depopulated through charge-transfer transitions near these crossings.

Surprisingly, the CAD channel in CD^+ was only observed for the lower-energy (798-nm) photons used in this study, despite the fact that half as many 392-nm photons are needed to reach the CAD state. This experimental finding is investigated further after establishing (below) the possible dissociation paths and mechanisms leading to CAD.

Two main mechanisms have been proposed for CAD (see, e.g., Refs. [32–34,37]). In the first the molecule is first ionized and then falls apart on states of the dication, while in the other the cation is excited to a dissociative state, stretches, then is ionized and finally dissociates into a doubly charged and a neutral fragment. More specifically, to determine the likely dissociation path(s) leading to $C^{2+} + D$, we use our measured KER-$\cos\theta$ distribution, shown together with the KER and $\cos\theta$ projections in Fig. 8. These spectra were measured for 22-fs, 798-nm pulses at a peak intensity of 6.3×10^{15} W/cm². For the CD^{2+} molecule to dissociate via the CAD channel, the laser must couple population to either the $2\,^2\Sigma^+$, $3\,^2\Sigma^+$, or $2\,^2\Pi$ state (see Fig. 7). Charge-transfer transitions between them may then lead to $C^{2+} + D$, i.e., the CAD channel, associated with the $3\,^2\Sigma^+$ state at large internuclear separation. Mixing of the $2\,^2\Sigma^+$, $3\,^2\Sigma^+$, and $2\,^2\Pi$ states, caused by radial and rotational coupling [78] inherent to CD^{2+} [75], can cause charge transfer even without the presence of the laser field. This
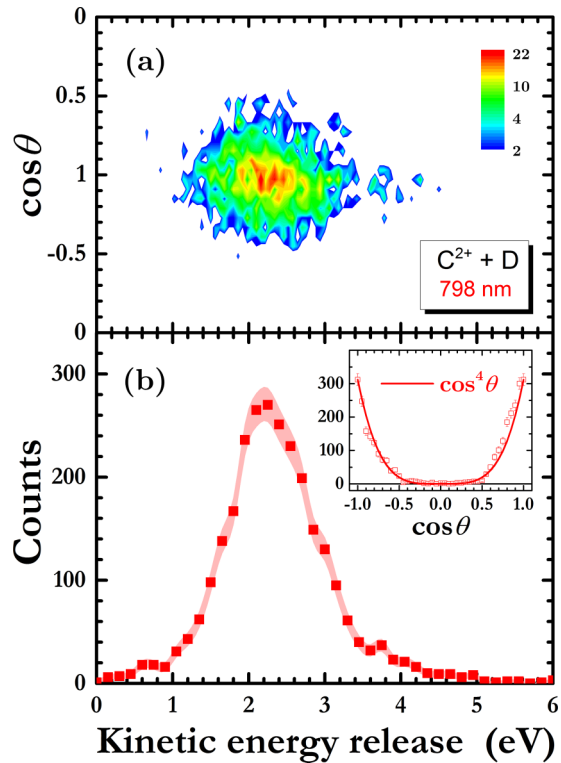
FIG. 8. (Color online) The measured spectra for CAD, namely, CD^+ breakup into $C^{2+} + D$ in 22-fs pulses at 798 nm and peak intensity of 6.3×10^{15} W/cm^2: (a) KER-$\cos\theta$ density plot, (b) KER distribution integrated over all angles (the shaded area represents the statistical errors), and (inset) angular distribution integrated over all KER. Note that CAD is strongly aligned along the laser polarization.

adds to the complexity of determining the explicit dissociation route, especially if the laser pulse is long enough in comparison to the propagation time to the curve crossing by the dissociating wave packet.

One pathway leading to CAD is initiated by ionization to the $2\,^2\Sigma^+$ state of CD^{2+}. The measured KER, shown in Fig. 8, suggests that dissociation on the $2\,^2\Sigma^+$ PEC to the $C^{2+} + D$ limit has to start at $R_i \simeq 2.8$–3.8 a.u., assuming no KER gain before ionization. Mixing of the $2\,^2\Sigma^+$ and $3\,^2\Sigma^+$ states is predicted to occur by radial coupling over an internuclear distance range that overlaps the one suggested by the measured KER. Specifically, the radial coupling between these states peaks at 3.2 a.u. and is significant for $R_i \simeq 2.3$–4 a.u. [75]. Alternatively, the slow dissociating wave packet on the $2\,^2\Sigma^+$ PEC can undergo a charge-transfer transition driven by rotational coupling near the avoided crossing at $R_c = 19.4$ a.u. Specifically, this involves $2\,^2\Sigma^+ \to 2\,^2\Pi \to 3\,^2\Sigma^+$ transitions (similar to those invoked by Gu *et al.* [75]) to explain charge-transfer transitions in $C^{2+} + H$ collisions leading to $C^+ + H^+$). Finally, laser-driven transitions between the $2\,^2\Sigma^+$ and $3\,^2\Sigma^+$ states at large internuclear separation can also yield the measured KER. However, classical calculations indicate that stretching on the $2\,^2\Sigma^+$ PEC from R_i to R_c takes about 32 fs, and by then the laser intensity of the 22-fs pulse has dropped by two orders of magnitude from its peak value, where ionization is assumed to occur. This reduces the importance of laser-induced transitions between these two

states, but one cannot completely rule out this mechanism. In contrast, laser-driven $2\,^2\Sigma^+ \to 3\,^2\Sigma^+$ (or $2\,^2\Pi$) transitions at smaller internuclear distances ($R_i \simeq 2.8$–3.8 a.u.), when the laser intensity is high, result in a KER much greater than that measured and therefore can be excluded as possible pathways. The latter argument also excludes direct ionization to the $3\,^2\Sigma^+$ and $2\,^2\Pi$ states, over the same range of internuclear distances, as likely pathways.

In contrast, ionization to the $3\,^2\Sigma^+$ or $2\,^2\Pi$ states at larger internuclear distances, marked by the yellow area in Fig. 7, provides another group of possible pathways to CAD, as the KER expected for $R_i \simeq 5.2$–10.6 a.u. is in agreement with the measured values under the assumption that the KER gained before ionization is relatively small. One specific route of this kind may involve, for example, excitation of the CD^+ from its ground electronic state to the $2\,^1\Sigma^+$ state (see Fig. 3) early in the pulse, followed by ionization of the stretched CD^+ ($R_i \simeq 5.2$–10.6 a.u.) to either the $3\,^2\Sigma^+$ or $2\,^2\Pi$ state. The KER gained during dissociation on the $2\,^1\Sigma^+$ PEC is estimated to be about 0.8 eV (a value consistent with the measured KER of the $C + D^+$ dissociation channel of CD^+), which combined with the KER gained on the $3\,^2\Sigma^+$ PEC from $R_i \simeq 9$ a.u. yields the average measured KER (2.3 eV). Other excited states of CD^+ may participate in such a mechanism involving ionization around $R_i \simeq 5.2$–10.6 a.u., but these routes cannot be distinguished from each other by the present measurements. It is important to note that ionization to the $3\,^2\Sigma^+$ state leads adiabatically to CAD. In contrast, ionization to the $2\,^2\Pi$ state requires a $2\,^2\Pi \to 3\,^2\Sigma^+$ transition driven by rotational coupling (see Ref. [75]). The same rotational-coupling mechanism can deplete CAD by driving $3\,^2\Sigma^+ \to 2\,^2\Pi$ transitions [75].

In short, our data support two possible mechanisms leading to CAD of CD^{2+}. The first involves ionization to the $2\,^2\Sigma^+$ at relatively short internuclear distances followed by either radial or rotational coupling transitions ending on the $3\,^2\Sigma^+$ state. The second is a two-step process, initiated by excitation of CD^+, followed by stretching and ionization to the $3\,^2\Sigma^+$ or $2\,^2\Pi$ state. Rotational coupling plays a key role in depleting or enhancing CAD of the $3\,^2\Sigma^+$ and $2\,^2\Pi$ states, respectively.

Now that the possible pathways leading to CAD are known, we return to the intriguing experimental observation mentioned before: namely, the unexpected absence of the CAD channel in our measurements employing the higher-energy (392-nm) photons, despite being measured when using the less-energetic (798-nm) photons at similar laser intensities. This is counterintuitive as one would expect multiphoton processes requiring a smaller number of photons to dominate at the same laser intensity.

It is well known that pulse duration can play an important role in the dissociation dynamics of molecules [43,79,80], and previous studies show that CAD dissociation channels are no exception [34]. The shortest 392-nm pulses available for this study were chirped 50-fs (FWHM) pulses while the 798-nm FTL pulses were 22 fs long, i.e., significantly shorter. To explore if the pulse duration may be responsible for the disappearance of the CAD channel, the data measured with 22-fs FTL pulses at 798 nm were compared to the data acquired with these FTL pulses chirped to 50 fs—using both positive and negative chirp while maintaining the same peak

intensity (3×10^{15} W/cm^2). No CAD signal was observed for the chirped 50-fs pulses, independent of chirp sign used. These findings suggest that the absence of CAD in the 392-nm measurements is most likely due to pulse duration and not the shorter wavelength. One may speculate that transitions around R_c between the states leading to the CAD or CSD channels may be affected by the longer laser pulses leading to the observed CAD suppression, but further work is needed to clarify the CAD-suppression mechanism. Future experiments using shorter (< 50 fs) pulses at 392 nm and several other wavelengths are required to further investigate this phenomenon. Alternatively, carefully designed pump-probe measurements can be used to turn the laser field on or off during the wave packet passage through the crossing at R_c. Such measurements, however, are still a challenge for molecular-ion targets due to their typically low target density.

IV. SUMMARY

In summary, we have presented an experimental method that improves the quality of 3D momentum imaging of laser-induced fragmentation of heteronuclear molecules with significant mass asymmetry. A CD$^+$ molecular ion was used to demonstrate the capabilities and limitations of this method. In addition, we have implemented this method to study the dissociation and dissociative ionization of a CD$^+$ beam in intense ultrashort laser pulses.

In particular, the most likely dissociation pathways leading to C$^+$ + D or C + D$^+$ have been identified based on the measured kinetic energy release and angular distributions. In addition we have explored the charge-asymmetric dissociation of CD^{2+} produced by ionizing the CD$^+$ target. Surprisingly this channel, namely the breakup into C^{2+} + D, is not visible when using frequency doubled photons at the same peak intensity as the 798-nm pulses. We show that the most likely reason for this curious phenomenon is the longer pulse duration of the 392-nm pulses, as increasing the pulse duration of the fundamental 798 nm leads to the same result.

[1] S. Backus, C. G. Durfee III, M. M. Murnane, and C. H. Kapteyn, Rev. Sci. Instrum. **69**, 1207 (1998).

[2] M. Protopapas, C. H. Keitel, and P. L. Knight, Rep. Prog. Phys. **60**, 389 (1997).

[3] P. H. Bucksbaum, A. Zavriyev, H. G. Muller, and D. W. Schumacher, Phys. Rev. Lett. **64**, 1883 (1990).

[4] A. Zavriyev, P. H. Bucksbaum, H. G. Muller, and D. W. Schumacher, Phys. Rev. A **42**, 5500 (1990).

[5] P. Agostini, F. Fabre, G. Mainfray, G. Petite, and N. K. Rahman, Phys. Rev. Lett. **42**, 1127 (1979).

[6] R. R. Freeman, P. H. Bucksbaum, H. Milchberg, S. Darack, D. Schumacher, and M. E. Geusic, Phys. Rev. Lett. **59**, 1092 (1987).

[7] *Atoms in Intense Laser Fields*, edited by M. Gavrila (Academic, San Diego, CA, 1992), and references therein.

[8] G. G. Paulus, W. Becker, W. Nicklich, and H. Walther, J. Phys. B: At., Mol. Opt. Phys. **27**, L703 (1994).

[9] M. J. Nandor, M. A. Walker, and L. D. V. Woerkom, J. Phys. B: At., Mol. Opt. Phys. **31**, 4617 (1998).

[10] A. Zavriyev, P. H. Bucksbaum, J. Squier, and F. Saline, Phys. Rev. Lett. **70**, 1077 (1993).

[11] A. Giusti-Suzor, X. He, O. Atabek, and F. H. Mies, Phys. Rev. Lett. **64**, 515 (1990).

[12] M. F. Kling, C. Siedschlag, A. J. Verhoef, J. I. Khan, M. Schultze, T. Uphues, Y. Ni, M. Uiberacker, M. Drescher, F. Krausz *et al.*, Science **312**, 246 (2006).

[13] M. Kremer, B. Fischer, B. Feuerstein, V. L. B. de Jesus, V. Sharma, C. Hofrichter, A. Rudenko, U. Thumm, C. D. Schröter, R. Moshammer *et al.*, Phys. Rev. Lett. **103**, 213003 (2009).

[14] B. Fischer, M. Kremer, T. Pfeifer, B. Feuerstein, V. Sharma, U. Thumm, C. D. Schröter, R. Moshammer, and J. Ullrich, Phys. Rev. Lett. **105**, 223001 (2010).

[15] T. Rathje, A. M. Sayler, S. Zeng, P. Wustelt, H. Figger, B. D. Esry, and G. G. Paulus, Phys. Rev. Lett. **111**, 093002 (2013).

[16] N. G. Kling, K. J. Betsch, M. Zohrabi, S. Zeng, F. Anis, U. Ablikim, B. Jochim, Z. Wang, M. Kübel, M. F. Kling *et al.*, Phys. Rev. Lett. **111**, 163004 (2013).

[17] A. Giusti-Suzor, F. H. Mies, L. F. DiMauro, E. Charron, and B. Yang, J. Phys. B: At., Mol. Opt. Phys. **28**, 309 (1995).

[18] J. H. Posthumus, Rep. Prog. Phys. **67**, 623 (2004).

[19] I. Ben-Itzhak, in *Progress in Ultrafast Intense Laser Science IV*, edited by K. Yamanouchi, A. Becker, R. Li, and S. L. Chin, Springer Series in Chemical Physics Vol. 91 (Springer, New York, 2009), p. 67.

[20] B. Gaire, J. McKenna, M. Zohrabi, K. D. Carnes, B. D. Esry, and I. Ben-Itzhak, Phys. Rev. A **85**, 023419 (2012).

[21] I. Ben-Itzhak, P. Q. Wang, J. F. Xia, A. M. Sayler, M. A. Smith, K. D. Carnes, and B. D. Esry, Phys. Rev. Lett. **95**, 073002 (2005).

[22] I. Ben-Itzhak, P. Q. Wang, J. F. Xia, A. M. Sayler, M. A. Smith, J. W. Maseberg, K. D. Carnes, and B. D. Esry, Nucl. Instrum. Methods Phys. Res., Sect. B **233**, 56 (2005).

[23] K. Sändig, H. Figger, and T. W. Hänsch, Phys. Rev. Lett. **85**, 4876 (2000).

[24] V. S. Prabhudesai, U. Lev, A. Natan, B. D. Bruner, A. Diner, O. Heber, D. Strasser, D. Schwalm, I. Ben-Itzhak, J. J. Hua *et al.*, Phys. Rev. A **81**, 023401 (2010).

[25] A. Natan, U. Lev, V. S. Prabhudesai, B. D. Bruner, D. Strasser, D. Schwalm, I. Ben-Itzhak, O. Heber, D. Zajfman, and Y. Silberberg, Phys. Rev. A **86**, 043418 (2012).

[26] M. Odenweller, N. Takemoto, A. Vredenborg, K. Cole, K. Pahl, J. Titze, L. P. H. Schmidt, T. Jahnke, R. Dörner, and A. Becker, Phys. Rev. Lett. **107**, 143004 (2011).

[27] F. Baumgartner and H. Helm, Phys. Rev. Lett. **104**, 103002 (2010).

[28] P. C. Fechner and H. Helm, Phys. Chem. Chem. Phys. **16**, 453 (2014).

[29] J. McKenna, A. M. Sayler, B. Gaire, N. G. Johnson, E. Parke, K. D. Carnes, B. D. Esry, and I. Ben-Itzhak, Phys. Rev. A **77**, 063422 (2008).

[30] M. V. Korolkov and K. Weitzel, J. Chem. Phys. **123**, 164308 (2005).

[31] A. M. Sayler, P. Q. Wang, K. D. Carnes, B. D. Esry, and I. Ben-Itzhak, Phys. Rev. A **75**, 063420 (2007).

[32] G. N. Gibson, M. Li, C. Guo, and J. P. Nibarger, Phys. Rev. A **58**, 4723 (1998).

[33] C. Guo, M. Li, and G. N. Gibson, Phys. Rev. Lett. **82**, 2492 (1999).

[34] N. G. Kling, J. McKenna, A. M. Sayler, B. Gaire, M. Zohrabi, U. Ablikim, K. D. Carnes, and I. Ben-Itzhak, Phys. Rev. A **87**, 013418 (2013).

[35] W. Eberhardt, E. W. Plummer, I. W. Lyo, R. Carr, and W. K. Ford, Phys. Rev. Lett. **58**, 207 (1987).

[36] K. Boyer, T. S. Luk, J. C. Solem, and C. K. Rhodes, Phys. Rev. A **39**, 1186 (1989).

[37] G. Gibson, T. S. Luk, A. McPherson, K. Boyer, and C. K. Rhodes, Phys. Rev. A **40**, 2378 (1989).

[38] Q. Liang, C. Wu, Z. Wu, M. Liu, Y. Deng, and Q. Gong, Int. J. Mass Spectrom. **286**, 28 (2009).

[39] C. Cornaggia, J. Lavancier, D. Normand, J. Morellec, and H. X. Liu, Phys. Rev. A **42**, 5464 (1990).

[40] H. Liu, Z. Yang, Z. Gao, and Z. Tang, J. Chem. Phys. **126**, 044316 (2007).

[41] V. Tagliamonti, H. Chen, and G. N. Gibson, Phys. Rev. A **84**, 043424 (2011).

[42] C. Guo, Phys. Rev. A **73**, 041401 (2006).

[43] P. Q. Wang, A. M. Sayler, K. D. Carnes, J. F. Xia, M. A. Smith, B. D. Esry, and I. Ben-Itzhak, Phys. Rev. A **74**, 043411 (2006).

[44] B. Gaire, J. McKenna, N. G. Johnson, A. M. Sayler, E. Parke, K. D. Carnes, and I. Ben-Itzhak, Phys. Rev. A **79**, 063414 (2009).

[45] The frequency resolved autocorrelation (FRAC) measurements were conducted using a Femtometer autocorrelator (from FemtoLaser, http://www.femtolasers.com/FEMTOMETER-TM.120.0.html). The pulse duration of 22 fs (FWHM in intensity) was determined by fitting a Gaussian to the fringe pattern envelope as explained in the user manual (see, e.g., Ref. [46]). An error of about 2 fs was estimated from a sample of independent measurements.

[46] J.-C. M. Diels, J. J. Fontaine, I. C. McMichael, and F. Simoni, Appl. Opt. **24**, 1270 (1985).

[47] Using the JRML laser known as PULSAR—a KM-Labs laser providing 2-mJ, down to 21-fs FTL pulses at a 10 kHz repetition rate with a central wavelength of about 790 nm.

[48] R. W. Boyd, *Nonlinear Optics* (Academic, New York, 1992).

[49] V. Krylov, A. Rebane, A. G. Kalintsev, H. Schwoerer, and U. P. Wild, Opt. Lett. **20**, 198 (1995).

[50] A. Sayler, Ph.D. thesis, Kansas State University, 2008.

[51] I. Ben-Itzhak, in *Fragmentation Processes: Topics in Atomic and Molecular Physics*, edited by C. T. Whelan (Cambridge University Press, Cambridge, 2013), p. 26.

[52] B. Gaire, Ph.D. thesis, Kansas State University, 2011.

[53] B. Gaire, U. Ablikim, M. Zohrabi, S. Roland, K. D. Carnes, and I. Ben-Itzhak (unpublished).

[54] Z. Amitay, D. Zajfman, P. Forck, U. Hechtfischer, B. Seidel, M. Grieser, D. Habs, R. Repnow, D. Schwalm, and A. Wolf, Phys. Rev. A **54**, 4032 (1996).

[55] U. Hechtfischer, J. Rostas, M. Lange, J. Linkemann, D. Schwalm, R. Wester, A. Wolf, and D. Zajfman, J. Chem. Phys. **127**, 204304 (2007).

[56] Z. Amitay, A. Baer, M. Dahan, J. Levin, Z. Vager, D. Zajfman, L. Knoll, M. Lange, D. Schwalm, R. Wester *et al.*, Phys. Rev. A **60**, 3769 (1999).

[57] S. Green, P. S. Bagus, B. Liu, A. D. McLean, and M. Yoshimine, Phys. Rev. A **5**, 1614 (1972).

[58] R. P. Saxon, K. Kirby, and B. Liu, J. Chem. Phys. **73**, 1873 (1980).

[59] B. Levy, J. Ridard, and E. L. Coarer, Chem. Phys. **92**, 295 (1985).

[60] E. Y. Sidky and I. Ben-Itzhak, Phys. Rev. A **60**, 3586 (1999).

[61] J. Demaison and G. Wlodarczak, Struct. Chem. **5**, 57 (1994).

[62] A. Lubezky, L. Chechelnitsky, and M. Folman, J. Chem. Soc., Faraday Trans. **92**, 2269 (1996).

[63] G. Herzberg, *Molecular Spectra and Molecular Structure. IR and Raman Spectra of Polyatomic Molecules* (Van Nostrand Reinhold, New York, 1945), Vol. 2.

[64] X. He, O. Atabek, and A. Giusti-Suzor, Phys. Rev. A **38**, 5586 (1988).

[65] S.-I. Chu, J. Chem. Phys. **75**, 2215 (1981).

[66] The 392-nm photon energy is 0.055 eV higher than two 798-nm photons—a difference that has no significant impact on our measurements, so for simplicity it is neglected in the light-dressed-state figure and associated discussion.

[67] A. Hishikawa, S. Liu, A. Iwasaki, and K. Yamanouchi, J. Chem. Phys. **114**, 9856 (2001).

[68] K. Codling and L. J. Frasinski, J. Phys. B: At., Mol. Opt. Phys. **26**, 783 (1993).

[69] K. Codling, L. J. Frasinski, and P. A. Hatherly, J. Phys. B: At., Mol. Opt. Phys. **22**, L321 (1989).

[70] K. Codling, C. Cornaggia, L. J. Frasinski, P. A. Hatherlyt, J. Morellec, and D. Normandtand, J. Phys. B: At., Mol. Opt. Phys. **24**, L593 (1991).

[71] P. A. Hatherly, M. Stankiewiczt, K. Codling, L. J. Frasinski, and G. M. Cross, J. Phys. B: At., Mol. Opt. Phys. **27**, 2993 (1994).

[72] I. Ben-Itzhak, S. G. Ginther, and K. D. Carnes, Phys. Rev. A **47**, 2827 (1993).

[73] K. Wohrer, G. Sampoll, R. L. Watson, M. Chabot, O. Heber, and V. Horvat, Phys. Rev. A **46**, 3929 (1992).

[74] J. P. Nibarger, M. Li, S. Menon, and G. N. Gibson, Phys. Rev. Lett. **83**, 4975 (1999).

[75] J.-P. Gu, G. Hirsch, R. J. Buenker, M. Kimura, C. M. Dutta, and P. Nordlander, Phys. Rev. A **57**, 4483 (1998).

[76] R. Wetmore, R. K. Boyd, and R. L. Roy, Chem. Phys. **89**, 329 (1984).

[77] W. Koch, L. Bowen, T. Weiske, C. B. Lebrilla, T. Drewello, and H. Schwarz, Chem. Phys. Lett. **142**, 147 (1987).

[78] B. H. Bransden and C. J. Joachain, *Physics of Atoms and Molecules*, 2nd ed. (Prentice-Hall, New York, 2003).

[79] A. Rudenko, B. Feuerstein, K. Zrost, V. L. B. de Jesus, T. Ergler, C. Dimopoulou, C. D. Schröter, R. Moshammer, and J. Ullrich, J. Phys. B: At., Mol. Opt. Phys. **38**, 487 (2005).

[80] J. McKenna, A. M. Sayler, F. Anis, B. Gaire, N. G. Johnson, E. Parke, J. J. Hua, H. Mashiko, C. M. Nakamura, E. Moon *et al.*, Phys. Rev. Lett. **100**, 133001 (2008).